UC Berkeley
Consortium on Deburring and Edge Finishing

Title
Development of an Analytical Model for Drilling Burr Formation in Ductile Materials

Permalink
https://escholarship.org/uc/item/1cq5k23b

Authors
Kim, Jinsoo
Dornfeld, David

Publication Date
2002

Peer reviewed

eScholarship.org Powered by the California Digital Library
University of California

#105

Development of an Analytical Model for Drilling Burr Formation in Ductile Materials

Jinsoo Kim
Graduate Student

David A. Dornfeld
Professor, Fellow ASME

5100A Etcheverry Hall,
Department of Mechanical Engineering,
University of California, Berkeley,
Berkeley, CA 94720-1740

An analytical model for drilling burr formation was developed. The model holds for ductile materials that do not show catastrophic fracture during the plastic deformation of workpiece material for burr formation. The proposed burr formation mechanism was based on the observation of behavior of workpiece materials during drilling of low alloy steel. The model was based on the principle of energy conservation and metal cutting theory. Experimental validation was done, and the results showed good agreement with the model. Based on the model, the effects of several important parameters on burr formation were investigated. [DOI: 10.1115/1.1429937]

1 Introduction

Most machining processes produce burrs. The term burr is used to indicate the presence of material at workpiece edges which was not there prior to machining operations. This material sometimes appears as a short mound of material and sometimes as a long thin projection [1,2]. The existence of a burr may reduce the fit of components in assembly, may injure workers during production, can be a source of small particles (debris from the burrs) inside a component, and may reduce the fatigue life of a component. Therefore, it is usually necessary to remove the burr (deburring). As a result, a lot of research has been done on deburring processes and research is still on going to improve and automate these processes. Relatively less attention has been given to the burr formation mechanism itself, although an understanding of the burr formation mechanism is essential in order to reduce deburring cost by reducing burr formation.

The drilling process produces burrs on both entrance and exit surfaces of a workpiece. An entrance burr forms on the entrance surface as the material near the drill undergoes plastic flow. The exit burr is the material extending off the exit surface of the workpiece. Since the exit burr is much larger than the entrance burr, most of the burr related problems mentioned above occur due to the exit burr. Therefore, most drilling burr-related studies have focused on the exit burr, and so does this study.

Drilling burr formation is quite a complex phenomenon influenced by many parameters. Previous researches showed that material property, drill geometry, and process condition are among the most important parameters [2–9]. Other minor variables, such as machine stiffness, temperature distribution near cutting edges, and use of coolant etc., also influence burr formation to some extent.

Most of the burr-related studies reported in the literature were experimental work. A competent analytical model can provide a more detailed understanding of the burr formation mechanism as well as the effects of related parameters. However, development of a reliable analytical model for drilling burr formation is challenging, due to the complexity of the drilling process itself and the excess in number of parameters to be considered. Lack of complete material property information is another hurdle as detailed material property depending on temperature and strain rate is very difficult to obtain. As a result, there is no generally accepted analytical model for drilling burr formation.

Contributed by the Materials Division for publication in the JOURNAL OF ENGINEERING MATERIALS AND TECHNOLOGY. Manuscript received by the Materials Division August 7, 2000; revised manuscript received August 8, 2001. Associate Editor: A. M. Rajendran.

Finite Element Analysis can be considered as an alternative choice for burr study and has been successfully applied to drilling burr formation [10–12]. This is for very limited conditions and more work on this needs to be done.

The purpose of this study is to propose an analytical model for burr formation in drilling ductile materials. The term "ductile material" here was used to indicate that there is no catastrophic fracture during burr formation before initial fracture occurs near the outer cutting edges of a drill. This considerably simplifies the problem, and holds for generally used low and medium alloy steel and stainless steel.

2 Observation of Drilling Burr Formation

The drilling burr has various shapes and size depending on the influencing parameters mentioned above. Figure 1 shows some examples of drilling burrs observed in drilling several materials. The left-hand pictures of each row represent burrs produced in relatively low feed and cutting speed, while right-hand pictures are for high feed and speed. When the feed and the cutting speed are low, the drilling burr tends to have a uniform shape along the hole periphery for most materials. The material property of workpiece makes a big difference when the feed and the cutting speed increase. When the material has moderate ductility, the material tends to elongate to some extent during burr formation, resulting in a large burr height and burr volume, Figs. 1(*a*), (*b*) and (*c*). However, if the material is quite brittle, catastrophic fracture occurs as the feed and the speed increases, resulting in irregular burrs having several large chunks, lobes, or petals as shown in Fig. 1(*d*).

Drawing kinematics of drilling burr formation gives us more insight into the burr formation mechanism. Even though the final burr shapes can look alike, the burr formation mechanism can be substantially different. Figure 2 shows proposed burr formation mechanisms for several burr shapes, matched with corresponding pictures observed by a high-speed video while drilling low alloy steel, AISI 1018 from [13]. The uniform burr has a relatively small and uniform burr height and thickness around the hole periphery. A drill cap may or may not be formed in the final step of drilling depending on the material ductility, drill geometry and process condition. The crown burr has large and nonuniform burr height.

As the drill approaches the work exit surface, the material under the chisel edge begins to deform. The distance from the exit surface to the point at which the deformation starts depends mainly on the thrust force during drilling. As the drill advances, the plastic deformation zone expands from the center to the edge of the drill. At the final step, the remaining material is bent and

 Copyright © 2002 by ASME

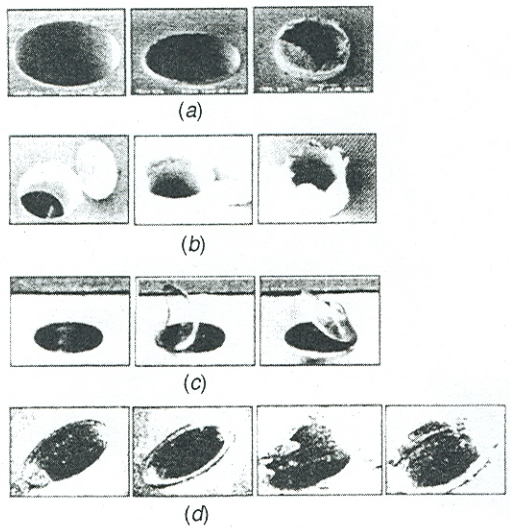

Fig. 1 Burr shapes observed in drilling metals [5,8,9]. (*a*) Low alloy steel 4118, (*b*) Stainless steel 304L, (*c*) Titanium alloy Ti-6Al-4V, (*d*) Al 6061.

pushed out ahead of the drill to form the uniform burr with a drill cap, Fig. 2(*a*). If the material does not have moderate ductility, plastic deformation is limited, and fracture occurs early at the center region of the drill. Continuous cutting occurs up to the final stage of drilling, creating a uniform burr but no drill cap, Fig. 2(*b*). A larger thrust force induces plastic deformation earlier in the process. The thicker material layer beneath the drill undergoes plastic deformation, and a larger maximum strain is induced at the center region of the exit surface. Therefore it is more likely that an initial fracture will occur at the center region of the exit surface, at the chisel edge, resulting in a crown burr. When there is considerable tool wear at the outer cutting edge of the drill, efficient cutting cannot be expected, and the material beneath the drill is pushed ahead rather than being cut. In this situation, there is a higher possibility of initial fracture occurring at the center region and creating a crown burr, Fig. 2(*c*) [8].

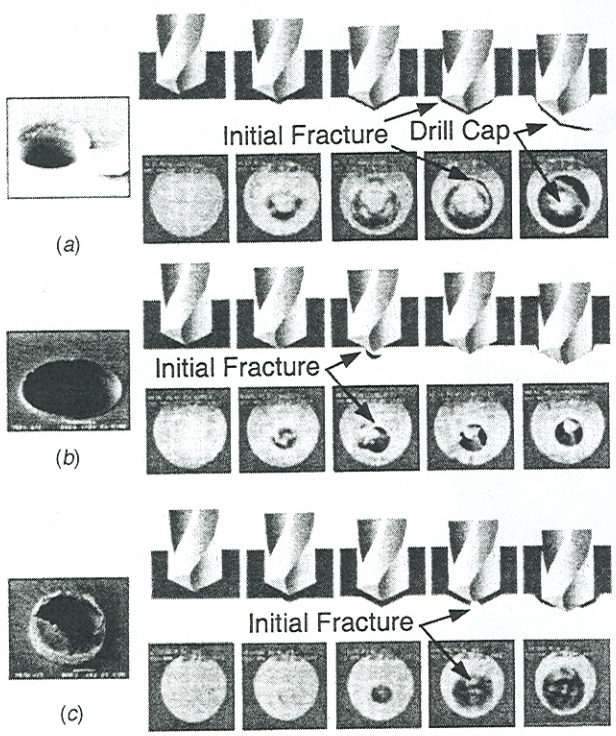

Fig. 2 Burr formation mechanisms matched with high-speed video pictures [8,13]. (*a*) Uniform burr with a drill cap, (*b*) uniform burr without a drill cap, (*c*) crown burr.

Very few researchers have attempted to develop an analytical model. Sofronas [14] proposed a pioneering analytical model which explains uniform burr formation without a drill cap, Fig. 2(*b*), by assuming that the chisel edge of a drill is through the workpiece first before plastic deformation starts. It uses an energy conservation method whereby the work done by the drilling force equals the work required to deform the remaining material beneath the drill. By assuming homogeneous material and perfectly plastic material behavior, the model calculates the initial material thickness that is to be a burr. Burr height and thickness were calculated by a volume conservation assumption.

The most common burr type for ductile material is the uniform burr with a drill cap. In most cases, with a reasonable combination of cutting conditions, initial fracture occurs at the outer cutting edge region, not near the drill center, creating a drill cap, as shown in Fig. 2(*a*).

In this study, an analytical model was developed to investigate the burr formation mechanism and predict the final burr size of the uniform burr with a drill cap.

3 Modeling of Drilling Burr Formation

3.1 Energy Conservation. A detailed proposed burr formation mechanism used for this study is shown in Fig. 3. No temperature effect, no strain rate effect, and no tool wear effect were considered. A perfectly plastic material model was used except for the material behavior at the shear plane.

As the drill advances toward the exit surface, part of material, hatched in the figure, starts to deform. It is assumed that the deformation is constrained within this part of the material. It is also assumed that no more cutting occurs in the deformed material after the deformation starts. The deformation continues until initial fracture occurs at the outer cutting edge, creating a uniform burr and a drill cap.

Before the "exit" deformation starts, all work provided by the drill is consumed in cutting the material (hole creation). However, after exit deformation starts, some part of the material, near the outer cutting edge region, is still being cut while the central part of the material is being deformed ahead of the drill without any cutting. At the final stage, Fig. 3(*d*), all work is only for material deformation without cutting. It is assumed here that total work, which consists of work done by the thrust force and work for material deformation, is constant from the initial material deformation, (*a*) to the final stage (*d*).

$$\Delta W_{th}+\Delta W_{df}=\Delta W_T=\text{Constant}$$
$$\Delta W_T-\Delta W_{th}=\Delta W_{df} \tag{1}$$

where, ΔW_{th}, ΔW_{df}, ΔW_T are work due to the thrust force of the drill, work for material deformation and total work, respectively, during the time period. The next step is to calculate each term of Eq. (1) and determine the resulting burr size.

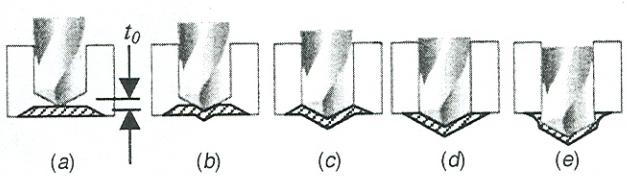

Fig. 3 Proposed burr formation mechanism

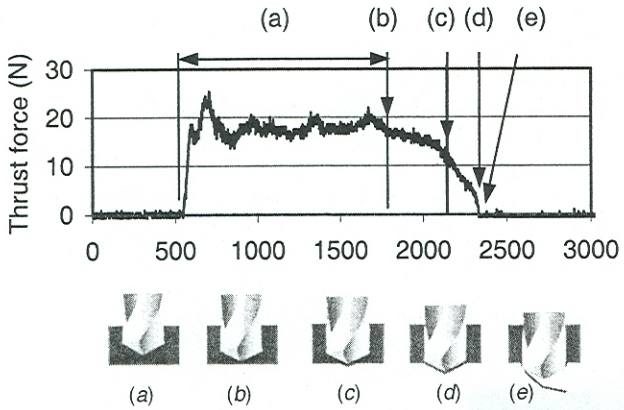

Fig. 4 Measurement of drilling thrust force matched with corresponding drilling stages. (*a*) Steady-state drilling, (*b*) deformation initiated, (*c*) chisel edge aligned with exit surface, (*d*) cutting finished, (*e*) fracture occurred.

3.2 Work Done by Drilling Force. In order to calculate ΔW_{th}, it is necessary to know the variation in thrust force during the time period as well as steady state thrust force before the deformation starts. For stainless steel AISI 304L with a split point twist drill, the thrust force during the whole drilling process was measured using a dynamometer. The drill diameter was 3.175 mm, the feed was 0.0317 mm/rev, and the rotational speed of the drill was 630 rpm. A uniform burr with a drill cap was created under these conditions. Figure 4 shows the measured force signal sampling at a rate of 100 Hz. The signal was matched with the corresponding stages of drilling from Fig. 3.

As shown in the figure, a constant thrust force is measured during the steady-state drilling. As the deformation of material starts, an abrupt decrease in thrust force is observed which continues until initial fracture occurs. The time period of interest in this study is from the point at which the exit deformation starts to the point at which the outer cutting edge of the drill is aligned with the exit surface. After that, no additional cutting occurs, and more material elongation and fracture create the burr and the drill cap.

No model is available explaining the behavior of the thrust force decrease in the final stage of drilling. From the force pattern observed in Fig. 4, and additional thrust force measurements carried out for different drill diameters and cutting conditions, it seems reasonable that the decrease of the thrust force follows a second-order polynomial pattern. In other words, the thrust force from the deformation initiation to the end of cutting can be represented as

$$F_{th}(y)=F_{th}\left(1-\frac{y^2}{(t_0+R/\tan p)^2}\right) \tag{2}$$

where, F_{th} is the steady-state thrust force, R is a drill radius, $2p$ is point angle and y is the distance of drill advancement measured from the deformation initiation point. Therefore,

$$\Delta W_{th}=F_{th}\int_0^L\left(1-\frac{y^2}{L^2}\right)dy,\quad L=\left(t_0+\frac{R}{\tan p}\right) \tag{3}$$

Calculation of steady-state thrust force should be a starting point in development of an analytical model for drilling burr formation. Many previous researchers proposed various models to calculate the thrust force during drilling [15–22]. Some of these models are purely empirical which holds only for a specific situation, while others are more general-purpose models. It was observed from the previous research that the typical formulation for drilling thrust force has the following form.

$$F_{th}=CH_b^{\alpha}f^{\beta}d^{\gamma} \tag{4}$$

where, α, β, γ are constants dependent upon material and drill geometry, f is feed, d is drill diameter and H_b is material hardness. C is a constant to be determined by calibration experiments. Development of an analytical model for drilling burr formation requires an expression for thrust force without necessity of the calibration experiment. In order to avoid the calibration experiment for thrust force prediction, the following is proposed.

Since the drilling process can be represented as an oblique cutting process which has changing oblique angles depending upon the relative radial position of the cutting edge, the theory of oblique cutting (modified from orthogonal cutting) can be applied.

The thrust force of orthogonal cutting process can be represented as [23]

$$F_{th}=\frac{t_1 W k_s \sin(\lambda-\alpha_n)}{\sin\phi\cos(\phi+\lambda-\alpha_n)} \tag{5}$$

where, t_1 is depth of cut, W is width of cut, k_s is shear strength of the workpiece material, λ is the friction coefficient between chip and tool face, ϕ is shear plane angle, and α_n is normal rake angle of tool. Assuming that the cutting edge of a drill is divided into a number of small segments, the elemental thrust force that acts on each segment is

$$\Delta F_{th}=\frac{f\sin p k_s\sin(\lambda-\alpha_n)}{2\sin\phi\cos(\phi+\lambda-\alpha_n)}\Delta W \tag{6}$$

where, f is the feed, and ΔW is the length of the segment being considered. The shear plane angle can be estimated from the Merchant equation as

$$\phi=\frac{\pi}{4}+\frac{(\alpha_n-\lambda)}{2} \tag{7}$$

No independent method of measuring the friction coefficient is available at this time. However, an analysis of published data relating cutting tests indicated that the friction angle can be assumed independent of cutting speed and related to the normal rake angle, α_n by the equation

$$\lambda=A+\frac{\alpha_n}{2} \tag{8}$$

where, A is a constant, and assumed 30 deg [24]. Combining Eqs. (6), (7), and (8) gives

$$\phi=\frac{\pi}{6}+\frac{\alpha_n}{4} \tag{9}$$

$$\Delta F_{th}=\frac{f}{2}\sin p k_s\frac{\sin\left(\frac{\pi}{6}-\frac{\alpha_n}{2}\right)}{\sin\left(\frac{\pi}{6}+\frac{\alpha_n}{4}\right)\cos\left(\frac{\pi}{3}-\frac{\alpha_n}{4}\right)}\Delta W \tag{10}$$

For any two fluted twist drill with a helix angle, δ_0, web thickness ratio, w, the normal rake angle across the main cutting edge is given by the following equation [25].

$$\alpha_n=\tan^{-1}\left\{\frac{\tan\delta_0(\rho^2-w^2\sin^2 p)-w\sin p\cos p}{\sin p(\rho^2-w^2)^{1/2}}\right\} \tag{11}$$

where, ρ is relative radius, r/R, which is the ratio of the distance, from the drill center to the segment, to the drill radius.

Rake angle by definition is an angle formed between the perpendicular line to the cutting velocity direction and the rake face of a tool. Unlike orthogonal cutting, the feed in drilling has to be considered in determining the rake angle, since the final cutting velocity direction changes with the distance from the drill center. Therefore a "dynamic rake angle," α_d, was defined as follows and used instead of the normal rake angle of Eq. (10) [19].

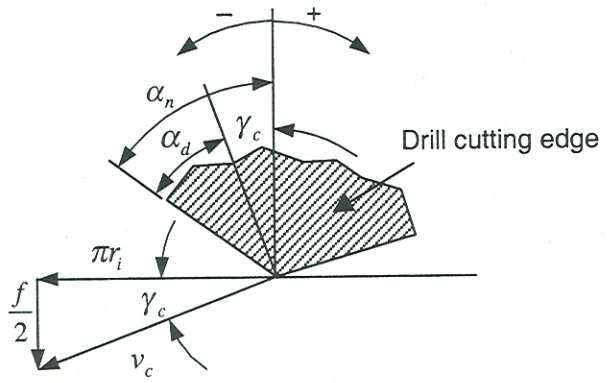

Fig. 5 Dynamic rake angle

$$\alpha_d = \alpha_n + \gamma_c = \alpha_n + \tan^{-1}\left(\frac{f}{2\pi r_i}\right) \tag{12}$$

where, r_i is the distance from the drill center to the element being considered, Fig. 5. It should be noticed that γ_c is always positive, and α_n can be either positive or negative.

Shear strength of material at the shear plane, k_s, is another challenge in calculating thrust force since it greatly changes depending on strain, shear rate, temperature, and cutting direction, etc. This is one of the reasons that most previous models require calibration tests. Ignoring the effects mentioned above, and assuming that tensile and shear strength of the material have same strain-hardening behavior,

$$k_s \approx \tau_u : \frac{\tau_u}{\tau_y} = \frac{\sigma_u}{\sigma_y} \tag{13}$$

where, σ_y, σ_u are tensile yield and ultimate strength, respectively, and τ_y, τ_u are shear yield and ultimate shear strength of material. From the octahedral shear stress relation when, $\sigma_1 = \sigma_2 = 0$, and $\sigma_1 = \sigma_y$

$$\tau_y = \frac{\sqrt{2}}{3}\sigma_y \tag{14}$$

Since the drill has two flutes, combining Eqs. (10)–(14) gives the expression for thrust force in drilling as follows,

$$F_{th} = \frac{\sqrt{2}}{3} R f\left(\frac{\sigma_u}{\sigma_y}\right) \cdot \sigma_y \cdot \sum_{i=1}^{N} \left\{ \frac{\sin\left(\frac{\pi}{6} - \frac{\alpha_d}{2}\right)(\rho_{i+1} - \rho_i)}{\sin\left(\frac{\pi}{6} + \frac{\alpha_d}{4}\right)\cos\left(\frac{\pi}{3} - \frac{\alpha_d}{4}\right)} \right\} \tag{15}$$

where, N is the number of segments along a cutting edge of the drill. Equation (15) assumes that efficient cutting occurs along whole length of the drill cutting edges. This assumption is reasonable for a split point twist drill, since it has secondary cutting edges near the chisel edge region. The rake angle of the secondary cutting edge of the split point twist drill can be treated as a constant, close to 0 degree. But for a conventional chisel edge drill, which has a very large negative rake angle near the drill center, efficient cutting cannot be expected, and an indentation model should be used for the chisel edge region [19].

In order to validate the thrust force model developed, an experimental validation was conducted. The thrust force was measured by a dynamometer (Kistler 9271A) during drilling stainless steel, AISI 304L with split point twist drills, and the results were compared with the values calculated by the model. The point angle for the drills was 135 deg, and σ_y, σ_u for the material were 281.6 MPa, 620.7 MPa, respectively. Table 1 shows the experimental conditions and corresponding thrust forces measured and calculated.

Table 1 Measured and calculated thrust fore

d (mm)	δ_0 (deg)	w	f (mm/rev)	Spindle speed (rpm)	Thrust force (N)	
					Measured	Calculated
3.18	22	0.425	0.0317	630	17.630	15.012
3.18	22	0.425	0.0317	1260	14.570	
3.18	22	0.425	0.0635	630	26.605	29.283
3.18	22	0.425	0.0635	1260	34.000	
3.18	22	0.425	0.1587	630	71.200	68.674
3.18	22	0.425	0.1905	630	83.960	80.823
3.97	25	0.380	0.0397	504	26.745	23.066
3.97	25	0.380	0.0397	1080	20.050	
3.97	25	0.380	0.0794	504	34.255	44.959
3.97	25	0.380	0.0794	1080	45.440	
3.97	25	0.380	0.2381	504	98.725	123.746
4.76	27	0.400	0.0476	420	36.030	32.320
4.76	27	0.400	0.0476	840	31.600	
4.76	27	0.400	0.0952	420	49.085	63.002
4.76	27	0.400	0.0952	840	64.120	

Since the Merchant model, on which the model was developed here, does not consider the cutting speed, calculated thrust forces do not reflect the cutting speed changes. However, as seen in the table, doubling the cutting speed induces less than 30% change in thrust force, while a change in feed rate induces at least 50%, to more than 100% change. Generally, the measured and the calculated values show good agreement, and the thrust force model developed so far is used for the rest of the analysis.

3.3 Work for Material Deformation. Work for material deformation during the time period of interest can be explained with a circular thin plate deformed into a circular cone shell. Figure 6 shows the half cross-section of the shape before deformation, $\square agcd$ and after deformation, $\square egbh$.

Deformation of $\square agcd$ to $\square egbh$ can be assumed to consist of following steps.

(I) Material elongation: $\square abcd \rightarrow \square hbck$
(II) Material bending along $\overline{bc}$
(III) Material bending along $\overline{bg}$

It is obvious that shear strain is also involved in the deformation. However, it is believed the shear strain is limited into very small region around the drill center, and the work done by the shear strain is negligible compared to the others since the thickness of the deformed material is very small compared to the drill radius, $R/t_0 \approx 50$.

The two bending deformations occur simultaneously. By the two bending deformations, it is assumed that point c moves to

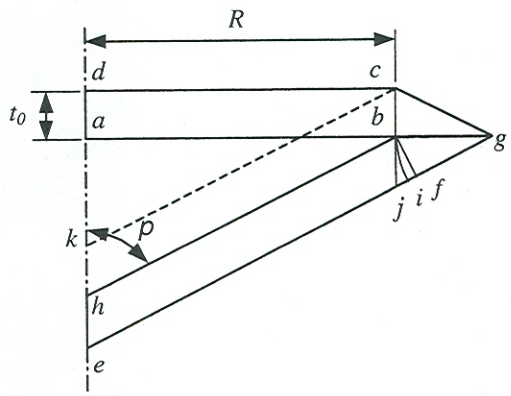

Fig. 6 Half cross-section of material beneath the drill before and after deformation

point b, and point b moves to point i. To simplify further calculation, point i is replaced by point f, since $\overline{if}$ is very small compared to the other dimensions. Therefore,

$$\Delta W_{df}=\Delta W_I+\Delta W_{II}+\Delta W_{III} \tag{16}$$

The strain distribution along $\overline{ab}$ is required to find ΔW_I, and can be represented as

$$\varepsilon_{\overline{ab}}=\ln\left(\frac{R/\sin p+\overline{ji}}{R}\right)=\ln\left(\frac{R/\sin p+t_0\sin p\cos p}{R}\right) \tag{17}$$

since $\overline{ji}\approx\overline{jf}$, $\overline{jf}=\overline{jb}\cos p$, and $\overline{jb}=t_0\sin p$ by the volume conservation of plastic deformation. However, it is known that the strain distribution due to deformation is not uniform but a function of radial distance from the center, highest at the center and decreasing outward [13]. Assuming that the strain distribution has the form of a second-order polynomial,

$$\varepsilon_{\overline{ab}}(r)=\frac{3}{2}\ln\left(\frac{1}{\sin p}+\frac{1}{2}\frac{t_0}{R}\sin 2p\right)\cdot\left(1-\frac{r^2}{R^2}\right) \tag{18}$$

Therefore,

$$\Delta W_I=\int_V\sigma_y\epsilon(r)\cdot dV$$

$$=\frac{3}{4}\pi R^2\sigma_y t_0\sin p\ln\left\{\left(\frac{1}{\sin p}\right)\cdot\left(1+\frac{t_0}{R}\sin^2 p\cos p\right)\right\} \tag{19}$$

where, V is the volume of deformed material. With perfectly plastic material model, and an approximation of

$$\ln\left\{\left(\frac{1}{\sin p}\right)\cdot\left(1+\frac{t_0}{R}\sin^2 p\cos p\right)\right\}$$

$$\cong\ln\left(\frac{1}{\sin p}\right)+\frac{t_0}{R}\sin^2 p\cos p$$

$$\text{since, }\frac{t_0}{R}\sin^2 p\cos p\ll 1 \tag{20}$$

the work for material elongation can be represented as

$$\Delta W_I=\int_V\sigma_y\epsilon(r)dV$$

$$=\frac{3}{4}\pi R^2 t_0\sigma_y\sin p\left\{\ln\left(\frac{1}{\sin p}\right)+\frac{t_0}{R}\sin^2 p\cos p\right\} \tag{21}$$

The work for the bending deformation along $\overline{bc}$ is

$$\Delta W_{II}=M_b\cdot\Delta\theta=\frac{1}{2}\pi\sigma_y\left(\frac{\pi}{2}-p\right)Rt_0^2 \tag{22}$$

where, M_b is the bending moment assuming perfect plastic material behavior, and $\Delta\theta$ is the angle of rotation of the bending deformation.

Similarly, the work for the bending deformation along $\overline{bg}$ is

$$\Delta W_{III}=M_b\cdot\Delta\theta=\sigma_y\int_0^{2\pi}\int_R^{R+1/2q}\left(R+\frac{1}{2}q-r\right)\cdot r\cdot dr\cdot d\theta$$

$$+\sigma_y\int_0^{2\pi}\int_{R+1/2q}^{R+q}\left(r-R-\frac{1}{2}q\right)\cdot r\cdot dr\cdot d\theta$$

$$=\frac{19}{12}\pi\sigma_y t_0^3\sin^3 p\tan^3 p \tag{23}$$

where, $q=t_0\sin p\tan p$. However, ΔW_{III} is negligible compared to the others since $t_0\ll R$. Therefore,

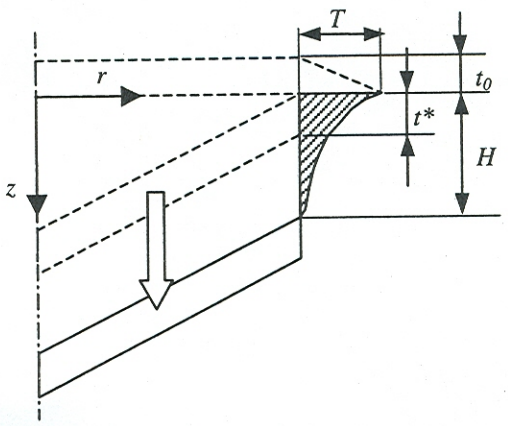

Fig. 7 Final burr formation and fracture

$$\Delta W_{df}\cong\Delta W_I+\Delta W_{II}=\frac{3}{4}\pi R^2 t_0\sin p\left\{\ln\left(\frac{1}{\sin p}\right)+\frac{t_0}{R}\sin^2 p\cos p\right\}$$

$$+\frac{1}{2}\pi\sigma_y\left(\frac{\pi}{2}-p\right)Rt_0^2 \tag{24}$$

3.4 Total Work. The total work, ΔW_T equals the product of the steady state thrust force and the distance from the deformation initiation point to the point at which the outer cutting edge of the drill is aligned the exit surface. That is,

$$\Delta W_T=F_{th}\left(t_0+\frac{R}{\tan p}\right) \tag{25}$$

3.5 Burr Formation and Burr Size Prediction. Combining Eqs. (1), (3), (15), (24), and (25), the initial thickness of deforming material beneath the drill, t_0, can be found by solving the following second-order polynomial equation, and used for burr size calculation.

$$t_0=\frac{1}{2X}(-Y+\sqrt{Y^2-4XZ})$$

$$X=\frac{3}{4}\pi\sin^3 p\cos p+\frac{1}{2}\pi\left(\frac{\pi}{2}-p\right)$$

$$Y=\frac{3}{4}\pi R\sin p\ln\left(\frac{1}{\sin p}\right)-\frac{\sqrt{2}}{9}f\left(\frac{\sigma_u}{\sigma_y}\right)\cdot\Phi \tag{26}$$

$$Z=-\frac{\sqrt{2}}{9}\frac{f}{\tan p}R\left(\frac{\sigma_u}{\sigma_y}\right)\cdot\Phi$$

$$\Phi=\sum_{i=1}^{N}\left[\frac{\sin\left(\frac{\pi}{6}-\frac{\alpha_d}{2}\right)(\rho_{i+1}-\rho_i)}{\sin\left(\frac{\pi}{6}+\frac{\alpha_d}{4}\right)\cos\left(\frac{\pi}{3}-\frac{\alpha_d}{4}\right)}\right]$$

Final burr formation and burr size predictions can be obtained by observing final deformation and fracture mechanisms, shown in Fig. 3 (*d*), (*e*) and redrawn in detail as shown in Fig. 7.

The hatched area represents the final burr shape with height, H and thickness, T. Thickness of deformed material, t^* can be found by volume conservation principle of plastic deformation, and can be represented as

$$t^*=t_0\sin p \tag{27}$$

It was observed that the final fracture for burr formation is similar to the fracture mechanism observed in tensile fracture of a material. With the cylindrical coordinate system shown in the figure, the volume conservation principle gives

$$dV=0, \quad d\varepsilon_\theta=0, \quad d\varepsilon_r=-d\varepsilon_z \tag{28}$$

And, effective plastic strain at the region of fracture is

$$\overline{\varepsilon_p}=\frac{2\sqrt{3}}{3}\varepsilon_z \tag{29}$$

When $\overline{\varepsilon_p}$ approaches the fracture strain of the material, ε_f, fracture occurs. Since,

$$\varepsilon_z=\ln\left\{\frac{H}{t^*}\right\}, \quad \epsilon_f=\ln\left\{\frac{100}{100-\%R.A.}\right\} \tag{30}$$

where, % R.A. is % reduction of area of material at tensile fracture, from Eq. (30), and geometric relation shown in the Fig. 7, burr height and thickness can be calculated by the following equations.

$$H=t_0 \sin p \exp\left\{\frac{\sqrt{3}}{2}\ln\left(\frac{100}{100-\%R.A.}\right)\right\}$$
$$T=t_0 \sin p \tan p \tag{31}$$

4 Experimental Validation and Discussion

Experiments were conducted to validate the analytical model developed. Two different materials, stainless steel, AISI 304L and low ally steel, AISI 4118, were selected for the validation test. Both materials have wide application as well as ductility moderate enough to produce uniform burrs in a general range of cutting conditions. Split point twist drills were used for the experiments, and two different drill diameters were used for each material. Table 2 shows the material properties of the materials, and Table 3 shows geometric specifications of the drills used for the experiment.

Figure 8 and 9 show the burr sizes measured from the experiments and calculated by the model. Wide ranges of burr size were observed in the experiments for a fixed feed and are the result of cutting speed effects. As cutting speed increases, many uncontrollable parameters, such as tool wear, heat generation and strain rate effect of the material, affect the burr formation compared to the lower speed situation. The analytical model, however, does not explain the cutting speed effects since the model is based on the Merchant shear plane model, which also does not consider the cutting speed. However, for both materials, burr height and thickness distribution with feed shows good agreement, specially for low feed ranges where cutting speed effect is not empathized.

The model can be effectively used to investigate the effects of other influencing parameters, as shown in Fig. 10. Figure 10 shows burr height and thickness variation within a range of one parameter while holding the other parameters at the values shown in Table 4. For example, Fig. 10(*a*) shows burr size increase with

Table 2 Material properties (produced by material manufacturer)

Material	Yield Strength (MPa)	Tensile Strength (Mpa)	% Reduction of Area
AISI 304L	281.6	620.7	72
AISI 4118	389.5	580.8	70

Table 3 Drill geometry

Material	Drill diameter (mm)	Point angle (deg)	Helix angle (deg)	Web thickness ratio
AISI 304L	1.984	135	19	0.38
	3.968	135	25	0.38
AISI 4118	4	135	25	0.2
	7	135	30	0.2

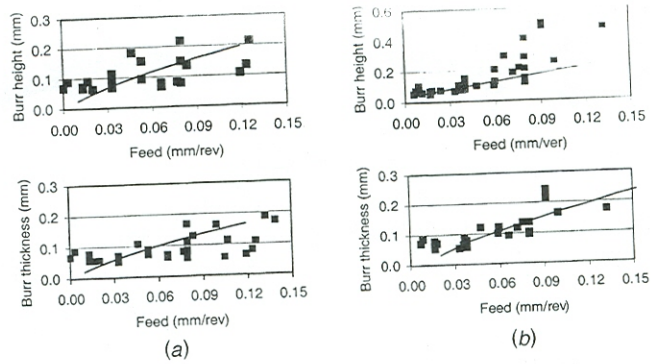

Fig. 8 Comparison of burr height and thickness between experiments and analysis in AISI 304L. (*a*) d=1.984 mm (*b*) d =3.968 mm ■ Experiments _____ Analysis.

point angle while all other variables are constant. The behavior of burr size can be understood by recalling the burr formation mechanism, specially the effect of the thrust force. As the point angle increases, the effective rake angle decreases resulting in increased thrust force and increased material volume deformed into the burr. It is noticeable that an abrupt increase in burr size occurs around point angle of 150 degree, Fig. 10(*a*). Increased

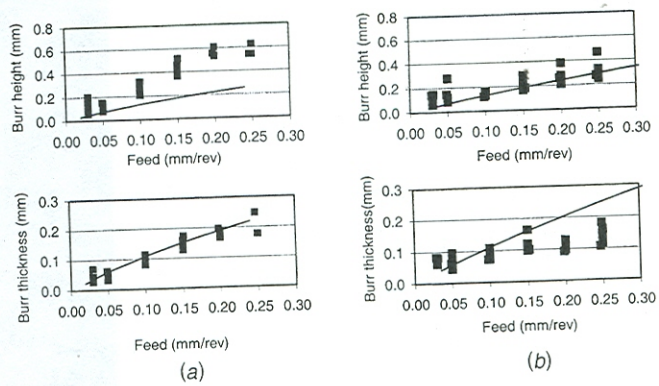

Fig. 9 Comparison of burr height and thickness between experimental measurement and analysis in AISI 4118. (*a*) d =4 mm (*b*) d=7 mm ■ Experiments _____ Analysis.

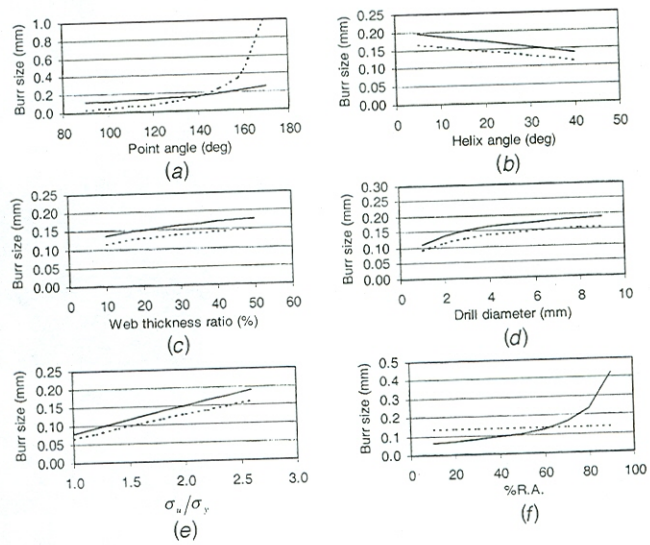

Fig. 10 Effects of various parameters on drilling burr size. ——Burr height ------- Burr thickness.

Table 4 Parameters used for analytical investigation

Drill diameter (mm)	3.968	Feed rate (mm/rev)	0.08	Helix angle (deg)	25
Point angle (deg)	135	Web thickness ratio	0.38	σ_u / σ_y	2.2

helix angle makes the effective rake angle increase, and the opposite effects in burr size occur from the increased point angle, Fig. 10(*b*). An increased web thickness ratio causes an increase in length of non-efficient cutting edge, resulting in an increased thrust force, Fig. 10(*c*). It is interesting to note that increase in drill diameter does not affect the burr size greatly, Fig. 10(*d*). Doubling the diameter from 4 mm to 8 mm causes only 10% increase in burr height. The ratio of σ_u / σ_y, and % R.A., Fig. 10 (*e*) and (*f*), indicate the strain hardening characteristics and the ductility of the material, respectively. As both parameters increase, the material undergoes larger plastic deformation before initial fracture occurs to form a burr, creating a larger burr.

5 Conclusions

Based on observation of drilling burr formation and physical principles, an analytical model was developed to predict drilling burr formation. The model is for ductile materials that produce a uniform burr with a drill cap.

- A formula to calculate the thrust force in a drilling process was developed. The formula was based on the Merchant shear plane model, and calculated thrust forces show good agreement with the measured values. Since the Merchant model does not include cutting speed effects, the thrust force model developed does not explain the difference in thrust force with cutting speed.
- An analytical model was successfully developed to predict the final drilling burr size. The model contains the effect of material property, drill geometry and process condition. It also contains several assumptions and simplifications. Burr sizes calculated by the model showed good agreement with experimental results. However, the model cannot be used to explain the cutting speed effects in drilling burr formation.
- Effects of other parameters on drilling burr formation were investigated with the model developed. The parameter effects are consistent with burr formation mechanism and the effects of thrust force in drilling.

Acknowledgments

The authors wish to thank the members of the Consortium on Deburring and Edge Finishing (CODEF) for their discussions, feedback, and financial support of this work.

References

[1] Gillespie, L. K., 1975, "Burrs Produced by Side-milling Cutters," Bendix Corporation Unclassified Topical Report, BDX-613-1303.

[2] Gillespie, L. K., 1975, "Burrs Produced by Drilling," Bendix Corporation Unclassified Topical Report, BDX-613-1248.

[3] Gillespie, L. K., 1976, "Effects of Drilling Variables on Burr Properties," Bendix Corporation, Unclassified Topical Report, BDX-613-1502.

[4] Link, R., 1992, "Gratbildung und Strategien zur Gratreduzierung" Ph.D dissertation, RWTH Aachen, Germany.

[5] Stein, J., and Dornfeld, D. A., 1995, "An Analysis of Burrs in Drilling Precision Miniature Holes Using a Fractional Factorial Design," ASME Symposium on Production Eng., Winter Annual Meeting.

[6] Pande, S., and Relekar, H., 1986, "Investigation on Reducing Burr Formation in Drilling," Int. J. Mach. Tool Des. Res., **26**, No. 3, pp. 339–348.

[7] Gillespie, L. K., and Blotter, P. T., 1976, "The Formation Properties of Machining Burrs," ASME J. Eng. Ind., **98**, No. 1, pp. 66–74.

[8] Kim, J., and Dornfeld, D. A., 2000, "Development of a Drilling Burr Control Chart for Stainless Steel," Transactions of NAMRI/SME, **XXVIII**, pp. 317–322.

[9] Dornfeld, D. A., Kim, J., Dechow, H., Hewson, J., and Chen, L. J., 1999, "Drilling Burr Formation in Titanium Alloy, Ti-6A1-4V," Annals of the CIRP V, **48/1**, pp. 73–76.

[10] Guo, Y. B., and Dornfeld, D. A., 1998, "Finite Element Analysis of Drilling Burr Minimization with a Backup Material," Transactions of NAMRI/SME, **26**, pp. 207–212.

[11] Guo, Y., and Dornfeld, D. A., 1998, "Integration of CAD of Drill with FEA of Drilling Burr Formation," Transactions of NAMRI/SME, **26**, pp. 201–206.

[12] Guo, Y., and Dornfeld, D. A., 2000, "Finite Element Modeling of Burr Formation Process in Drilling 304 Stainless Steel," ASME J. Manuf. Sci. Eng., to appear.

[13] Furness, R., 1998, *High Speed Video of Drilling Burr Formation*, AMTD, Ford Motor Company.

[14] Sofronas, A., 1975, "The Formation and Control of Drilling Burrs," Ph.D. dissertation, The University of Detroit.

[15] Chandrasekharan, V., Kapoor, S. G., and Devor, R. E., 1995, "A Calibration Procedure for Fundamental Oblique-Cutting Model Coefficients Based on A Three-Dimensional Mechanistic Drilling Force Model," Transactions of NAMRI/SME, **XXVII**, pp. 255–260.

[16] Chandrasekharan, V., Kapoor, S. G., and Devor, R. E., 1995, "A Mechanistic Approach to Predicting the Cutting Forces in Drilling: With Application to Fiber-Reinforced Composite Materials," ASME J. Eng. Ind., **117**, pp. 559–570.

[17] Chandrasekharan, V., Kapoor, S. G., and Devor, R. E., 1998, "A Mechanistic Model to Predict the Cutting Force System for Arbitrary Drill Point Geometry," ASME J. Manuf. Sci. Eng., **120**, pp. 563–570.

[18] Chen, Y. R., Ni, J., and Katz, Z., 2000, "A Compact Geometrical-Model-Based Force Model and Improved Material Calibration Procedure for Arbitrary Geometry," submitted for publication, CIRP Annals.

[19] Mauch, C., and Lauderbaugh, L. K., 1990, "Modeling the Drilling Process-An Analytical Model to Predict Thrust Force and Torque," Computer Modeling and Simulation of Manufacturing Processes, Singh, B., Im, Y., Haque, I., Altan, C., eds., ASME, New York, pp 59–66.

[20] Roadinger, T. J., and Townsend, M. A., 1980, "Torque and Thrust Parameters in Drilling Using Dimensional Analysis," ASME J. Eng. Ind., **102**, pp. 37–44.

[21] Rubenstein, C., 1991, "The Torque and Thrust Force in Twist Drilling-I. Theory," Int. J. Mach. Tools Manuf., **31**, No. 4, pp. 481–489.

[22] Rubenstein, C., 1991, "The Torque and Thrust Force in Twist Drilling-I. Comparison of Experimental Observations with Deductions from Theory," Int. J. Mach. Tools Manuf., **31**, No. 4, pp. 491–504.

[23] Merchant, M. E., 1945, "Basic Mechanics of the Metal Cutting Process," J. Appl. Phys., **16**, pp. 267–275.

[24] Williams, R. A., 1974, "A Study of Drilling Process," ASME J. Eng. Ind. **96**, pp. 1207–1215.

[25] Galloway, D. F., 1957, "Some Experiments on the Influence of Various Factors on Drill Performance," Trans. ASME, **79**, pp. 191–231.